



저작자표시-비영리-변경금지 2.0 대한민국

이용자는 아래의 조건을 따르는 경우에 한하여 자유롭게

- 이 저작물을 복제, 배포, 전송, 전시, 공연 및 방송할 수 있습니다.

다음과 같은 조건을 따라야 합니다:



저작자표시. 귀하는 원저작자를 표시하여야 합니다.



비영리. 귀하는 이 저작물을 영리 목적으로 이용할 수 없습니다.



변경금지. 귀하는 이 저작물을 개작, 변형 또는 가공할 수 없습니다.

- 귀하는, 이 저작물의 재이용이나 배포의 경우, 이 저작물에 적용된 이용허락조건을 명확하게 나타내어야 합니다.
- 저작권자로부터 별도의 허가를 받으면 이러한 조건들은 적용되지 않습니다.

저작권법에 따른 이용자의 권리는 위의 내용에 의하여 영향을 받지 않습니다.

이것은 [이용허락규약\(Legal Code\)](#)을 이해하기 쉽게 요약한 것입니다.

[Disclaimer](#)

Thesis for the Degree of Master of Engineering

**Luminescence Properties of Y_2WO_6 and
 $Y_2WO_6:Yb^{3+}/Er^{3+}$ crystals: Self-activation and
Upconversion**

Advisor: Prof. Hyo Jin Seo

by

Cuili Chen

Department of physics and Interdisciplinary Program of

Biomedical, Mechanical & Electrical Engineering

The Graduate School

Pukyong National University

August 2016

**Luminescence Properties of Y_2WO_6 and
 $Y_2WO_6:Yb^{3+}/Er^{3+}$ crystals: Self-activation and
Upconversion**

**Y_2WO_6 및 $Y_2WO_6:Yb^{3+}/Er^{3+}$ 결정의 자기 활성화 및
상방전환 형광특성 연구**

Advisor: Prof. Hyo Jin Seo

by

Cuili Chen

Department of physics and Interdisciplinary Program of
Biomedical, Mechanical & Electrical Engineering

The Graduate School

Pukyong National University

August 2016

Luminescence Properties of Y_2WO_6 and $\text{Y}_2\text{WO}_6:\text{Yb}^{3+}/\text{Er}^{3+}$ crystals: Self-activation and Upconversion

A dissertation

by

Cuili Chen

Approved by:

(Chairman: Professor Cheol Woo Park)

(Member: Ph.D. Kyoung Hyuk Jang)

(Member: Professor Hyo Jin Seo)

August 2016

Contents

Introduction	1
1. Background Theory	4
1.1 A general introduction of luminescence	4
1.2 Self-activation luminescence	4
1.3 Upconversion luminescence	6
2. Experiment Section	9
3.1 Initial Chemical Reagents and synthesis equipments	9
3.2 Preparation processes	10
3.3 Characterization	13
3.4 Optical measurement	14
3. Results and discussion	16
4.1 Luminescence properties of the Y_2WO_6 phosphor	16
4.1.1 Structure and morphology	16
4.1.2 Luminescence properties of Y_2WO_6	22
4.2 Upconversion luminescence of $Y_2WO_6:Yb^{3+}/Er^{3+}$	29
4.2.1 Morphology and structure	29
4.2.2 Luminescence properties	33
4.3 Upconversion properties of $Y_2WO_6:10\%Yb^{3+}/2\%Er^{3+}$	41
4.3.1 Structure and morphology	41
4.3.2 Luminescence properties	46
4. Conclusion	50
Acknowledgement	51
Published Paper	53
References	55

Luminescence Properties of Y_2WO_6 and $Y_2WO_6:Yb^{3+}/Er^{3+}$ crystals: Self-activation and Upconversion

Cuili Chen

Department of physics and Interdisciplinary Program of Biomedical, Mechanical &
Electrical Engineering

Pukyong National University

Abstract

Self-activation and upconversion luminescence properties of monoclinic tungstate Y_2WO_6 crystals were investigated optical and laser-excitation spectroscopy. The luminescence material of monoclinic Y_2WO_6 host and $Y_2WO_6:Yb^{3+}/Er^{3+}$ with various Er^{3+} concentration were synthesized via both classical solid state method and facile hydrothermal method. The sodium surfactant dodecyl benzene sulfonate (SDBS) was used to modify the samples to obtain the peculiar morphology during the hydrothermal synthesis process. The crystal structure of the Y_2WO_6 host and $Y_2WO_6:Yb^{3+}/Er^{3+}$ were characterized by X-ray diffraction (XRD) and their morphology features were measured by scanning electron microscopy (SEM). The monoclinic Y_2WO_6 host shows different

emitting color depending on different excitation wavelength due to the possession of two luminescence centers: W-O charge transfer and oxygen vacancy. The emission bands of Er^{3+} are obtained by excitation at 980 nm. The upconversion spectra of the samples were obtained under different excited power from which it is found that the slope values of the power dependent results decrease due to the cross relaxation process as the Er^{3+} doping concentration increases. The dominant upconversion mechanism of the monoclinic $\text{Y}_2\text{WO}_6:\text{Yb}^{3+}/\text{Er}^{3+}$ phosphor was further investigated according to the level structures of Yb^{3+} and Er^{3+} ions.

Introduction

The upconversion luminescence was predicted in 1950s and reported for the first time by Auzel for $\text{CaWO}_4: \text{Yb}^{3+}/\text{Er}^{3+}$ in 1966 [1]. The interest in significant phenomenon has increased due to the discovery of the possibility of its application [2-3]. The upconversion luminescence properties have been intensively investigated for the usage in the fields of optical energy and photodynamic therapy, photocatalytic materials, bio-makers, sensors and drug delivery system [4-5].

The upconversion luminescence is a type of special and classical anti-Stokes luminescence phenomenon which converts the long wavelength (low energy) to short wavelength (high energy), usually transfers from near infrared to visible or ultraviolet radiation. As the mechanism of upconversion process, two or more photons are absorbed through various approaches and then just one photon is emitted with higher energy [6]. The unique 4f electronic orbital in rare earth ions was shielded by 5d and 6s electronic level so that narrower the spectrum band, however, unfortunately the transition of shielded 4f electrons are forbidden by the parity selection rule. Therefore, an effective measure of energy transfer (ET) would be taken in order to enhance the absorption and emission intensity. In the case of upconversion luminescence, Yb^{3+} ions usually take a role of sensitizers for absorbing the near infrared light then transfer its absorbed energy to other acceptor ions. Such rare earth ions as Er^{3+} , Tm^{3+} or Ho^{3+} can be served as energy acceptors. The process

called energy transfer upconversion (ETU) in which the energy absorbed by sensitizers is sequentially transferred to acceptor [7]. Beyond that, another important energy migration approach named cooperative energy transfer (CET) in which two sensitizers must simultaneously transfer their energy to acceptor under the condition of the too large energy gap between ground and excited state, like Tb^{3+} ions [8-9].

Tungstate compounds present advantageous properties in chemical and physical stability as well as in diverse crystal morphologies. In addition, the vibration energy of chemical bonds in tungstates is relative low attributed to the possession of heavy metal ions in the crystal lattice. It is beneficial to obtain high quantum efficiency due to the matrices with low phonon energy.

Recently, some papers published about upconversion luminescence in the host of tungstates or molybdates. For example, $KY(MoO_4)_2: Yb^{3+}/Er^{3+}/Tm^{3+}/Ho^{3+}$ was investigated for color-tunable upconversion emission[10], $Gd_2(WO_4)_3:Er^{3+}$ for application of erbium upconverters to solar cells [11], $SrWO_4:Er^{3+}/Yb^{3+}$ [12] for the optical heating phosphor and $Gd_2(WO_4)_3:Er^{3+}/Yb^{3+}$ [13] for the color-tunable single-phased phosphors, $Gd_2(WO_4)_3:Er^{3+}/Yb^{3+}$ [14] for pumping-route-dependent concentration quenching and temperature effect. For the metrics of the monoclinic Y_2WO_6 , enhanced luminescence in $Sm^{3+}/Eu^{3+}/Dy^{3+}$ doped Y_2WO_6 microstructures through Gd^{3+} codoping has been reported by Kaczmarek et al [15]. And Ding et al has reported the tunable oxygen vacancy photoluminescence in Y_2WO_6 selectively occupying yttrium sites using

lanthanum [16]. However, detailed investigation about upconversion luminescence of $\text{Y}_2\text{WO}_6:\text{Yb}^{3+}/\text{Er}^{3+}$ has not been reported so far. Thus the work performed for the purposes that investigate luminescence mechanism and relaxation approaches. The samples $\text{Y}_2\text{WO}_6:\text{Yb}^{3+}/\text{Er}^{3+}$ were obtained with the fixed 10% Yb^{3+} concentration and various Er^{3+} concentration. The samples were systematically investigated through the analysis of structure, morphology and the luminescence properties.



1. Background Theory

1.1 A general introduction of luminescence

There is a long history that people try to acquire the light source except for the natural sun light. The incandescence and luminescence are two dominant routes in a material which emits light. The former one radiate light via all atoms and the latter only luminescence centers. The luminescence centers in inorganic crystal are created usually by addition of a trace amount of impurities or dopants. The rare earth elements play the valuable role as dopants in luminescence materials due to its peculiar chemical characteristics. It shares similar electronic structure of an incompletely filled 4f shell which is shielded from the surroundings by the $5s^2$ and $5p^6$ electrons. Therefore the effect of crystal field on the 4f electronic transition is small. Thus luminescent materials doped with rare earth ions have attracted considerable attention for the great potential in application [17-18].

The host lattice is the direct surroundings of the luminescence center so they are of prime importance in luminescence materials since the influence to the luminescence performance. The covalency and crystal field are main factors responsible for different spectral property [19-22].

1.2 Self-activation luminescence

The transition metal compounds such as vanadates, niobates and tungstates are important for luminescent materials which can be

self-activated. Examples are VO_4^{3-} , NbO_6^{7-} , NbO_4^{3-} , WO_4^{2-} and WO_6^{6-} . The transition occurs by the excitation from ligands (non-bonding orbital) to the d^0 ion (anti-bonding orbital) since the transition metal ions with an empty shell [23]. Their absorption and emission spectrum show the intense and broad band with a large Stokes shift after optical absorption ($\Delta R \gg 0$).

The position of absorption and emission bands is influenced by the factors as follow: (1) ionization potential, e.g. the absorption band of CaWO_4 is located at 250 nm, however, the CaMoO_4 at 290 nm. (2) The number of the ligands, e.g. CaWO_4 has the first absorption at 40000 cm^{-1} , that of Ca_3WO_6 is at 35000 cm^{-1} ; (3) mutually interaction between ions, e.g. Ca_3WO_6 with isolated WO_6^{6-} groups has its absorption band at 35000 cm^{-1} , that of WO_3 with connective WO_6^{6-} groups at a visible region.

Some structure types with special characteristics can promote luminescence efficiency, for examples, edge or face sharing of octahedral complexes like Li_3NbO_4 and $\text{Ba}_3\text{W}_2\text{O}_9$, and the occurrence of short metal-ligand distance such as $\text{CsNbOP}_2\text{O}_7$ and KVOF_4 .

The transition metal complex with empty d shell shows a long decay time of several hundred microseconds. Vander Waals et al. prove that the emitting state is a spin triplet. They showed also that excited state is strongly distorted due to the Jahn-Teller effect [24].

1.3 Upconversion luminescence

The process of upconversion refers to transferring the excited long wavelength (low energy) to emitted short wavelength (high energy) in the luminescence materials. The principle of upconversion is shown in Fig. 2.1. At first, the ion is excited from A to B. Then this ion will be further excited from B to C if the lifetime of energy level B is not too short. At last the emission from C to A may occur. The special anti-Stokes emission can be used as detecting infrared radiation visually.

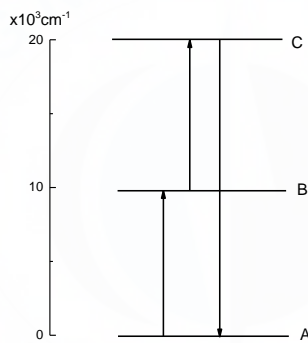


Fig. 2.1 The simplified principle of upconversion.

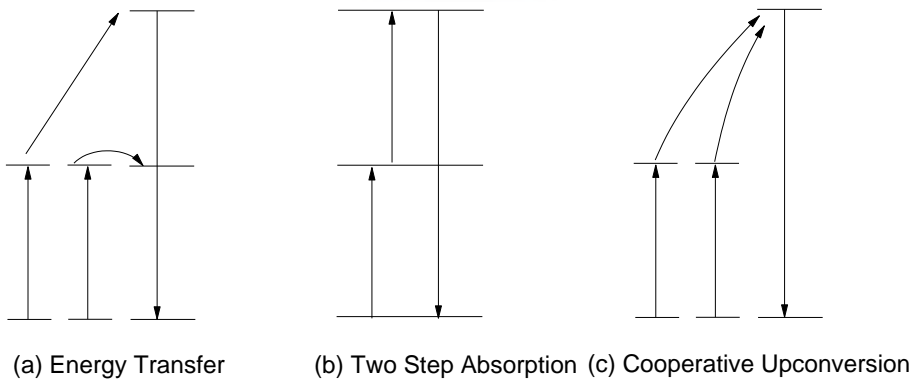


Fig. 2.2 The representative upconversion processes.

There are many upconversion mechanisms which show different conversion efficiencies. Higher-efficient processes require energy levels which are resonant between the incoming and outgoing radiations. Fig. 2.2 shows representative energy schemes. Fig. 2.2(a) shows energy transfer upconversion. The sensitizer transfer their excitation energy to another activators; Fig. 2.2 (b) shows two-step absorption process which needs only the activator ions; and Fig. 2.2 (c) shows cooperative upconversion which two sensitizers transfer simultaneously their excitation energy to activators without intermediate energy level.

Trivalent rare earth ions are very suitable for upconversion process since their rich intermediary levels. The Yb^{3+} ions have a substantially larger optical cross-section and a lesser tendency for concentration quenching in comparison with other rare-earth ions and the higher excitation densities can be realized. The absorbed energy can then be efficiently transferred to such ions as Er^{3+} or Tm^{3+} , giving rise to green and red or blue emission, respectively. For example, materials with Yb^{3+} and Er^{3+} can realize green emission from near-infrared excitation through the two-photon process. Another example is materials with Yb^{3+} and Tm^{3+} which convert the infrared into the blue emission by three-photon upconversion process. Except for trivalent rare earth ions, transition metal ions ($\text{MgF}_2:\text{Ni}^{2+}$) and $5f^n$ ions have also been observed the upconversion phenomenon.

Solid state materials doped rare earth ions for upconversion luminescence have been extensively investigated [2] [25]. As usual it can

be treated as the processes of excited state absorption (ESA) and energy transfer upconversion (ETU). For an upconversion process, the luminescence intensity (I_{uc}) is proportional to the pumping laser power density (P) according to the following equation [17]:

$$I_{uc} \propto P^n \quad \text{with } n=2,3,4,\dots$$

Where, n represents the number of pump photons absorbed as per high energy photon emitted. P is pumping power density of incident laser beam. The power density is calculated from the ratio between the laser power (W) and the area of the light spot (cm^2) on a sample surface. According to this relation, a slope n of the $\log(I_{uc})$ vs $\log(P)$ curve can be determined.

The most important application of infrared upconversion materials seems to be the detection of infrared light from laser diodes. Since the visible emissions generated from these materials are quadratically or cubically dependent upon excitation intensity, detection is particularly favorable for intense or focused laser light. Recently, the significant phenomenon has potential application in the fields of optical energy, photodynamic therapy, photocatalytic materials, bio-makers, sensors and drug delivery system. However, there are also negative aspects of upconversion. If we are interested in the luminescence or stimulated emission of intermediate level, upconversion will decrease the population of this level. This type of upconversion prevents a material from becoming a good laser.

2. Experiment Section

3.1 Initial Chemical Reagents and synthesis equipments

Table 3.1 A detailed list of the chemical reagents used during the experiment process.

No.	Reagent	purity	F.W.	Manufacturer
1	WO ₃	99.9%	231.84	SIGMA-ALDRICH. CHEMIE. GmbH
2	Y ₂ O ₃	99.99%	225.82	Shanghai Shanpu Chemical Led. China
3	Yb ₂ O ₃	99.9%	394.08	Wako. Pure Chemical Industries. Ltd
4	Er ₂ O ₃	99.99%	382.52	Shanghai Shanpu Chemical Led. China
5	Na ₂ WO ₄ ·2H ₂ O	Extra pure	239.85	DAEJUNG CHEMICALS & METALS co.Ltd
6	HNO ₃	60%	63.01	DAEJUNG CHEMICALS & METALS co.Ltd
7	SDBS	Chemical pure	348.48	DAEJUNG CHEMICALS & METALS co.Ltd
8	CH ₃ CH ₂ OH	99.5%	46.07	DAEJUNG CHEMICALS & METALS co.Ltd

As shown in table 3.1. A series of $Y_2WO_6:Yb^{3+}/Er^{3+}$ samples with 10% Yb^{3+} and various Er^{3+} doping concentration were synthesized via both classical solid state method and facile hydrothermal method. All of chemical reagents were used without further treatment.

Some equipments are necessary for the synthesis process as follows:

① muffle furnace; ② oven; ③ beaker; ④ alumina crucibles; ⑤ agate mortar; ⑥ Magnetic stirring electric jacket

3.2 Preparation processes

The sample $Y_2WO_6:Yb^{3+}/Er^{3+}$ was synthesized by simple solid-state reaction method using starting materials of Y_2O_3 (99.99%), WO_3 (99.9%), Yb_2O_3 (99.9%), and Er_2O_3 (99.99%). The concentration of Yb^{3+} was fixed to be 10 mol% and the activator Er^{3+} was set as 0, 1, 2, 5, 10, 15 and 20 mol%, which substitute for Y^{3+} in molar percentages. At first, all of starting reagents were mixed in stoichiometric ratios, added some ethyl alcohol as mixed medium, and then ground in an agate mortar for half an hour to obtain the homogeneous mixture. Secondly, the mixture was transferred into the alumina crucibles, and then calcined in the muffle furnace at 700°C for 5 hours in air. The obtained powder was thoroughly mixed again and increased to 1100 °C for 5h in air. The $Y_2WO_6:Yb^{3+}/Er^{3+}$ series were obtained after cooling down the samples to room temperature. The follow graph is as shown in Fig. 3.1.

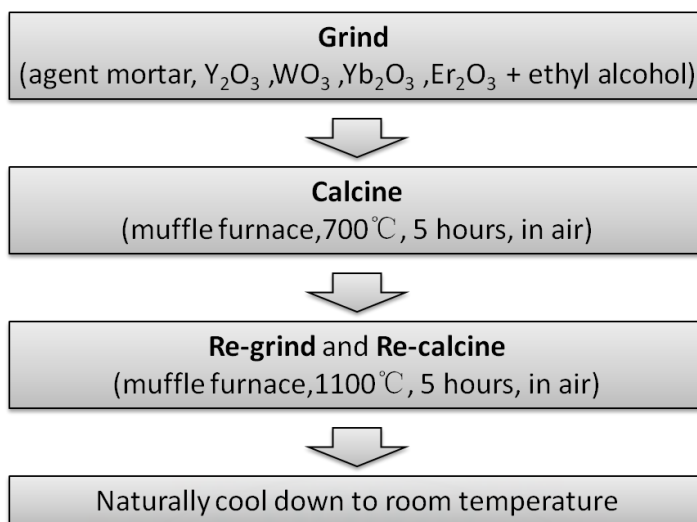


Fig. 3.1 The follow diagram of preparation process of Y₂WO₆:Yb³⁺/Er³⁺ through solid state method

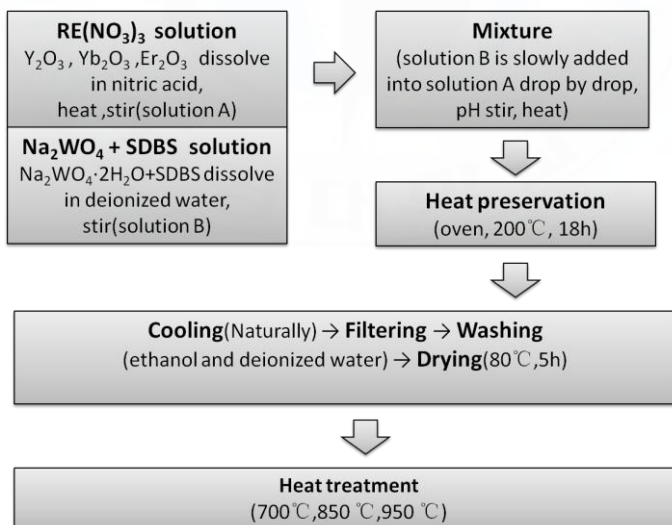


Fig. 3.2 The flow chart of preparation process of Y₂WO₆:Yb³⁺/Er³⁺ through hydrothermal method.

The sample of Y_2WO_6 host codoped with 10% Yb^{3+} and 2% Er^{3+} was also prepared by hydrothermal method in the presence of surfactant SDBS (sodium dodecyl benzene sulfonate). First, by dissolving the metal oxide (88% Y_2O_3 , 10% Yb_2O_3 , 2% Er_2O_3) with dropping the 60% nitric acid at 70 °C (heated by Magnetic stirring electric jacket) under stirring on a magnetic stirrer, 2 mmol rare earth $RE(NO_3)_3$ were obtained. Keep proper temperature to remove the redundant nitric acid. Second, 2 mmol $Na_2WO_4 \cdot 2H_2O$ was dissolved in 20 ml deionized water and 1 mmol SDBS was added under stirring. Then the Na_2WO_4 solution was slowly introduced into the $RE(NO_3)_3$ solution drop by drop with vigorous stirring. The pH value was controlled to neutral level via adding the dilute $NH_3 \cdot 2H_2O$. After 30 min, the 60 ml mixture was transferred into a autoclave (Teflon bottle held in a stainless steel), and maintained at 200 °C for 18 h in an oven. After that the autoclave was cooled to room temperature in the air. And the solid state precursors was obtained after filtering, washing (deionized water and ethanol, several times) and drying in air (80 °C, 5 h). Finally, the precursors annealed at 700, 850 and 950 °C to obtain the four samples. The preparation process of hydrothermal method is shown as Fig. 3.2.

All of the samples in this work were obtained through the two methods as mentioned above. Table 3.2 shows the detailed information of the $Y_2WO_6:Yb^{3+}/Er^{3+}$ series.

Table 3.2 A list of detailed information of the $Y_2WO_6:Yb^{3+}/Er^{3+}$ series.

No.	Doping concentration		Synthesis method
	Yb ³⁺ (%)	Er ³⁺ (%)	
1	0	0	Solid state
2	0	0	hydrothermal
3	10	0.01	Solid state
4	10	1	Solid state
5	10	2	Solid state
6	10	5	Solid state
7	10	10	Solid state
8	10	15	Solid state
9	10	2	hydrothermal

3.3 Characterization

The crystal structure of the sample series was confirmed by X-ray diffraction (XRD) patterns using Cu- K α (Philips XPert/MPD). The XRD data of 2θ range from 10° to 70° with a scanning rate of $4.0^\circ \text{ min}^{-1}$ and a scanning step size of 0.02° . The feature of morphology was observed through a field-emission scanning transmission electron microscopy (FE-SEM) (S-4800, Hitachi). Transmission electron microscopy (HR-TEM, JEOL JEM-2100F) was also used to observe the morphologies and microstructures.

3.4 Optical measurement

For the host sample Y_2WO_6 , the photoluminescence excitation/emission spectra (PL-PLE) were measured both at room temperature and low temperature. The excitation and emission spectra were measured by using a 450W Xenon lamp (150W) as a light source dispersed with a 25cm monochromator (Acton Research Corp. Pro-250). The emission from the sample was dispersed by a 75 cm monochromator (Acton Research Corp. Pro-750) and followed by feeding into a photomultiplier tube (PMT) (Hamamatus R928). To further clarify the luminescence mechanism of undoped tungstate lattice, the host crystal was refrigerated down in a closed cycle helium cryostat to a low temperature range from 7 K. A simple schematic diagram is showed as Fig. 3.3.

For the sample series of $Y_2WO_6:Yb^{3+}/Er^{3+}$, the upconversion emission spectra and power-dependence were measured. The samples were excited by the 980 nm continuous wave Laser Diode (LD). The filters (30% and 60% decreasing) were used to obtain the weak excited energy. The emission signal was dispersed by the 75 cm monochromator and observed with the PMT. A simple schematic diagram is shown in Fig. 3.4

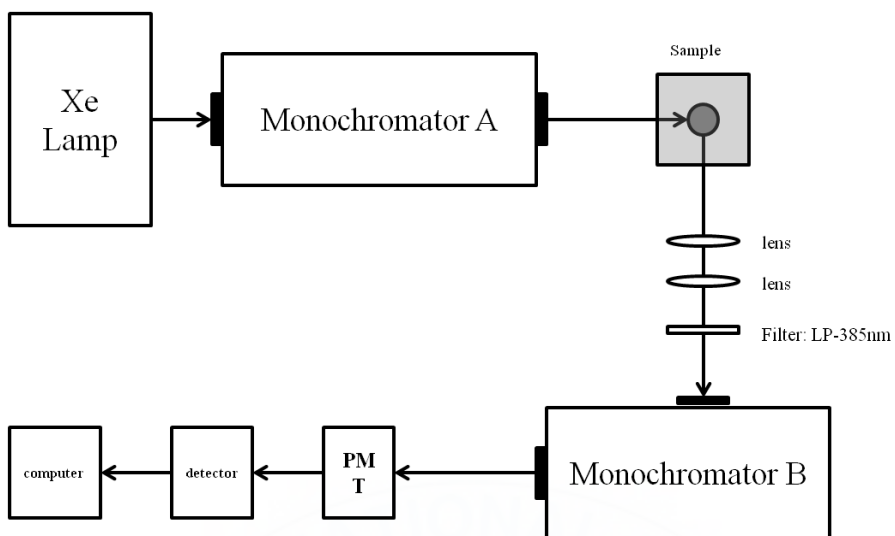


Fig. 3.3 The schematic map of the sample Y_2WO_6 measurements

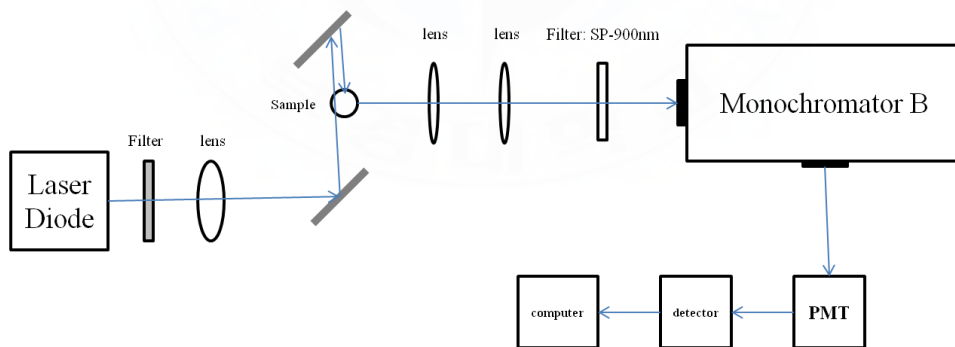


Fig. 3.4 The schematic map of upconversion measurements

3. Results and discussion

4.1 Luminescence properties of the Y_2WO_6 phosphor

4.1.1 Structure and morphology

Structure characterization of Y_2WO_6 host lattice. The yttrium tungstates Y_2WO_6 were synthesized through both the solid state and the hydrothermal methods. The crystal phase of the Y_2WO_6 particles was investigated by XRD measurements and the structure refinement was performed by the GSAS program. Fig. 4.1.1 (a) shows excellent crystalline Y_2WO_6 crystal synthesized by high temperature solid state method at 1200 °C. Fig. 4.1.1 (b) presents the XRD patterns of the samples prepared by the hydrothermal processes in a neutral pH solution. The results indicate that the final Y_2WO_6 products could not be synthesized directly in the solution and need to take heat treatment. Obviously, the hydrothermal precursors could not match well with standard PDF card (PDF#23-1489, found in JCPDS database). After heat treatment at 650 °C, most of the impurity peaks disappeared but all the peaks are weak and broaden. After heat treatment at higher temperature 1200 °C, the characteristic peaks of the XRD patterns for the monoclinic Y_2WO_6 phase can be distinguished, and no additional peaks are present.

The Y_2WO_6 phosphors are well crystallized in a monoclinic space group $P 1 2/c 1$ (13) with the unit cell parameters as follow: $Z=4$, $a=7.5847\text{\AA}$, $b=5.3307\text{\AA}$, $c=11.3536\text{\AA}$, $\beta=104.4224^\circ$; the cell ratio: $a/b=1.4228$, $b/c=0.4695$, $c/a=1.4969$; The cell volume: $V=444.58(3)\text{\AA}^3$.

The crystal structure sketch of monoclinic Y_2WO_6 is presented in Fig. 4.1.2, which was structured using the refined crystal phase data drawn by diamond 3.2 (software of Crystal and Molecular Structure Visualization).

All the W^{6+} ions in monoclinic Y_2WO_6 are coordinated by six non-equivalent O^{2-} ions to form the distorted octahedrons due to the different bond length. The detailed information about atomic parameters are shown in table 4.1.1.

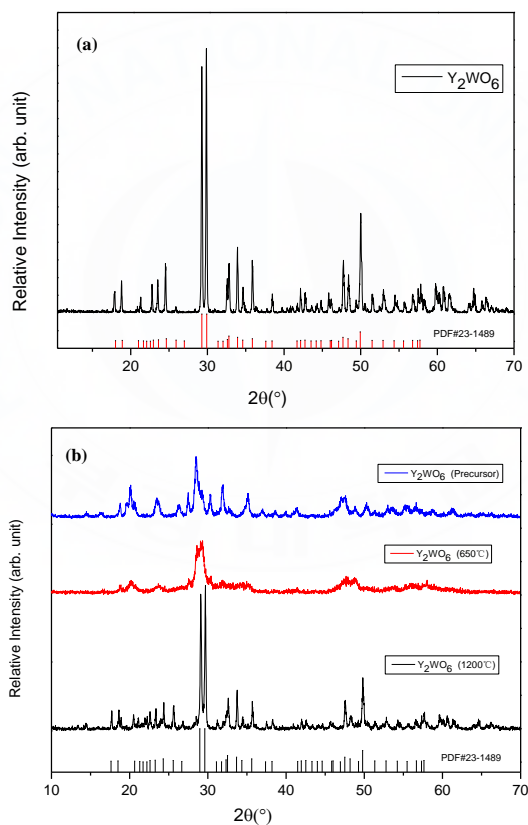


Fig. 4.1.1 XRD patterns of Y_2WO_6 crystal synthesized by solid state method (a); hydrothermal method (b).

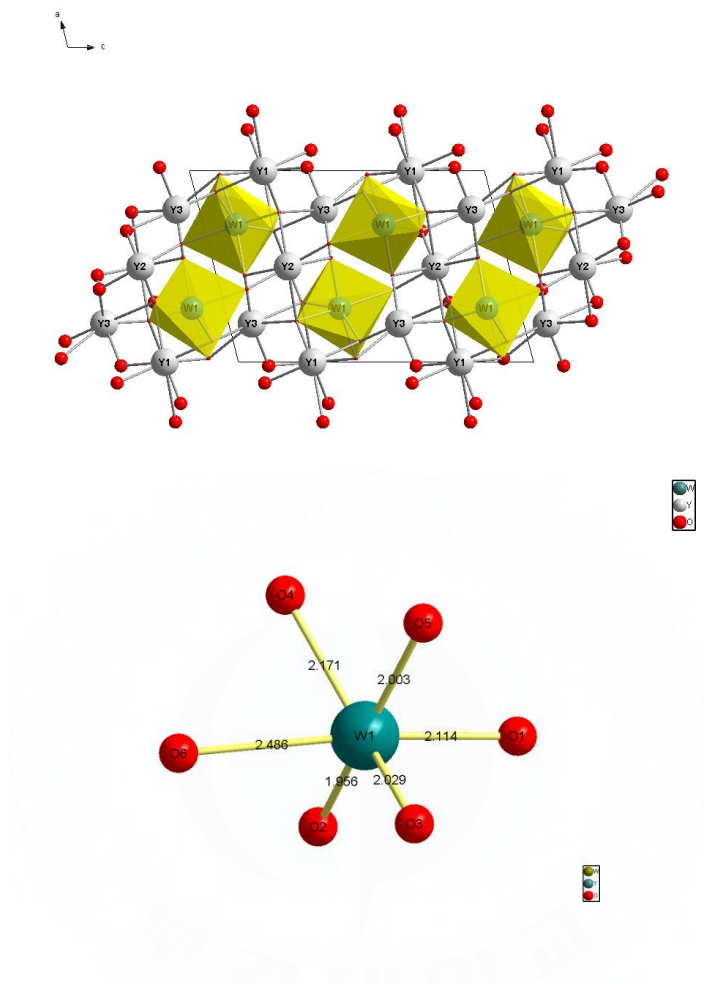


Fig. 4.1.2 Crystal structure of monoclinic Y_2WO_6 in the $P12/c1(13)$ space group.

Table 4.1.1 Refined atomic parameters of the Y_2WO_6 host lattice.

Atom	Wyck.	Site	x/a	y/b	z/c
W1	4g	1	0.28	0.25	0.39
Y1	2e	2	0	0.74	$\frac{1}{4}$
Y2	2f	2	$\frac{1}{2}$	0.69	$\frac{1}{4}$
Y3	4g	1	0.20	0.20	0.08
O1	4g	1	0.37	0.13	0.57
O2	4g	1	0.52	0.39	0.39
O3	4g	1	0.14	0.45	0.45
O4	4g	1	0.27	0.27	0.27
O5	4g	1	0.06	0.40	0.40
O6	4g	1	0.23	0.18	0.18

Atom	Wyck.	Site	x/a	y/b	z/c
W1	4g	1	0.28	0.25	0.39
Y1	2e	2	0	0.74	$\frac{1}{4}$
Y2	2f	2	$\frac{1}{2}$	0.69	$\frac{1}{4}$
Y3	4g	1	0.20	0.20	0.08
O1	4g	1	0.37	0.13	0.57
O2	4g	1	0.52	0.39	0.39
O3	4g	1	0.14	0.45	0.45
O4	4g	1	0.27	0.27	0.27
O5	4g	1	0.06	0.40	0.40
O6	4g	1	0.23	0.18	0.18

The Y^{3+} and W^{6+} ions in Y_2WO_6 are crystallographically ordered in such a way that the distorted WO_6 octahedrons are separated from each other by Y^{3+} ions rather than the WO_6^{6-} groups linked as chain or formed dimers. Thus every O^{2-} ions is shared by a W^{6+} ion and nearest neighboring Y^{6+} ions. The electron configuration of W^{6+} in the complexes shows its own feature with an empty d shell, which makes the electronic charge easy to move from oxygen ligands to the central metal ions W^{6+} as the crystal was excited by sufficient energy.

Morphology characterization of Y_2WO_6 host lattice. The microscopic structure of the samples was characterized by FE-SEM. Fig. 4.1.3 shows the typical FE-SEM photographs of both samples by solid state and hydrothermal (precursors, annealed samples). Figs. 4.1.3 (a) and (b) are the FE-SEM images of the precursors of the samples by hydrothermal method at different magnifications, which show the phosphors particles size less than $1 \mu m$ and exhibits schistose morphology. Normally, the samples with the schistose morphology lead to larger superficial area which will further influence other properties of the materials. Fig. 4.1.3 (c) shows microscopic morphology of the precursors annealed at $1200^\circ C$. As we see, some schistose particles melt together after annealing and the size of particles grew up to above $1\mu m$ but the size still less than the particle synthesized by solid state method. If we choose the annealing temperature lower to $950^\circ C$, the monoclinic phase also can be formed and can keep the particle size almost the same. At last Fig. 4.1.3 (c) shows

morphology of the samples synthesized by high temperature method, which shows approximate rhomb with clear edges and sizes are about a few micrometers.

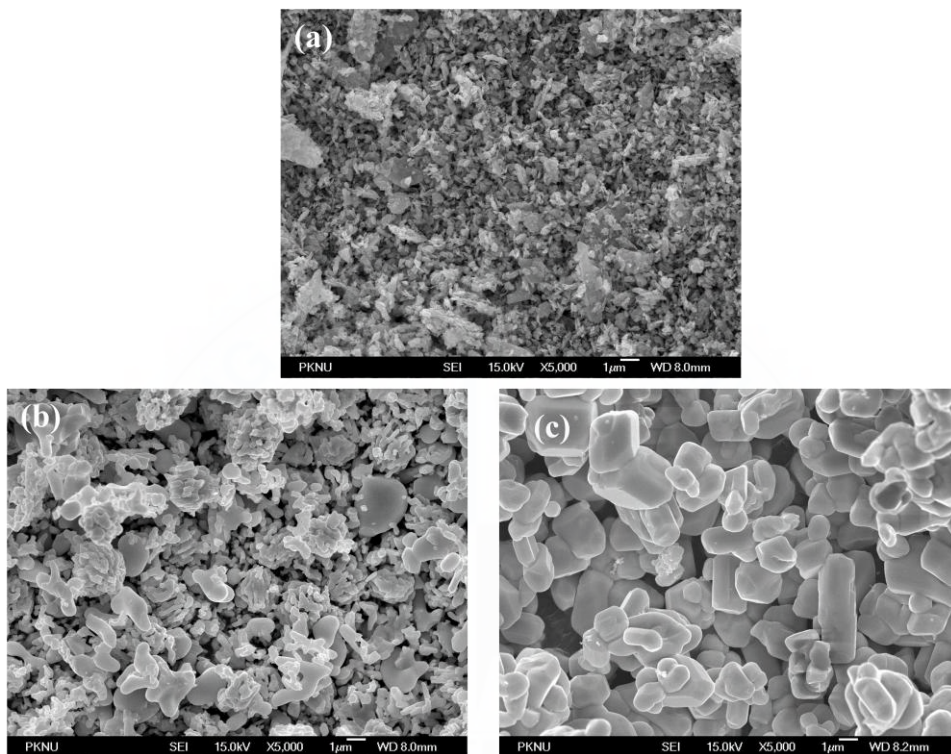


Fig.4.1.3 FE-SEM images of Y_2WO_6 synthesized by different method. (a)hydrothermal method samples (b) Annealed hydrothermal samples at $1200^\circ C$. (c) Samples synthesized by solid state method

4.1.2 Luminescence properties of Y_2WO_6

The PL and PLE spectra of the Y_2WO_6 host crystal at 7K are shown in Fig. 4.1.4. The excitation spectrum was obtained by monitoring the 490 nm luminescence and emission spectrum excited by 303 nm radiation. The PL and PLE spectra exhibit broad band corresponding to the charge transfer (CT) transition in the WO_6 groups. The broad band excitation in ranged from 220 to 380 nm peaking at 303 nm and the emission band is ranged from 380 to 700 nm peaking at 450 nm. At low temperature the clear double bands are observed in the PLE spectrum. They were decomposed into two components by the Gaussian function. The two Gaussian components of the excitation band are located at 301 nm (FWHM: 53 nm) and 345 nm (FWHM: 25 nm) and the emission bands are located at 441 nm (FWHM: 63 nm) and 486 nm (FWHM: 100 nm). The above results indicate that the self-activated emission of the Y_2WO_6 is attributed to the different types of luminescence centers.

The excitation spectrum of the 490 nm emission was also measured in the temperature range from 7 to 300 K as shown in Fig. 4.1.5. It is clear that there exist two components in the excitation spectrum at low temperature 7 and 100 K. The luminescence intensity is weaker at room temperature than that at 7 K. The strongest luminescence intensity is observed at 100 K.

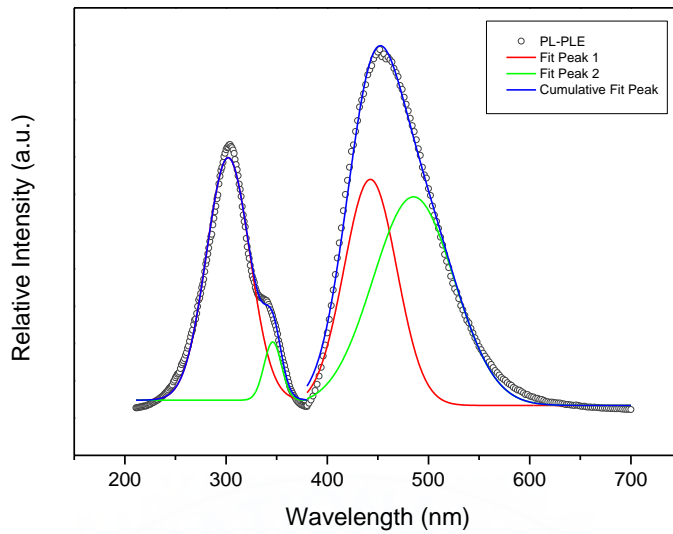


Fig.4.1.4 PL/PLE spectrum. Excitation spectrum monitored by 490 nm and emission spectrum excited by 303 nm of Y_2WO_6 host lattice measured at 7 K.

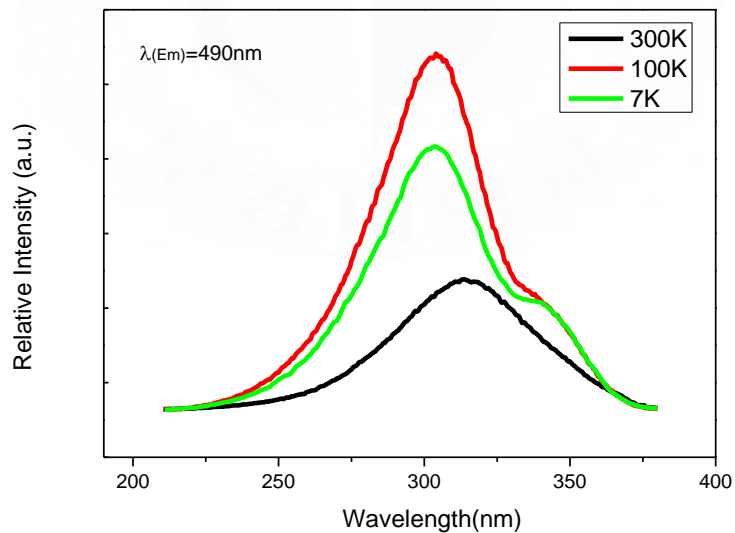


Fig.4.1.5 Excitation spectrum of Y_2WO_6 crystal phosphor monitored by 490nm at the temperature of 7, 100 and 300 K.

Different excitation wavelength was chosen to excite the different luminescence center. The emission spectrum measured in the temperature range from 7 to 300 K as shown in Fig. 4.1.6. The insets show the photographs for the emitting color distinction when excited by different wavelength. The emission spectrum excited by 303 nm exhibits peak wavelength located at 460 nm (see Fig. 4.1.6 (a)) while emission peak at 500 nm excited by 337 nm. But no change in spectral feature is observed for excitation at low temperature.

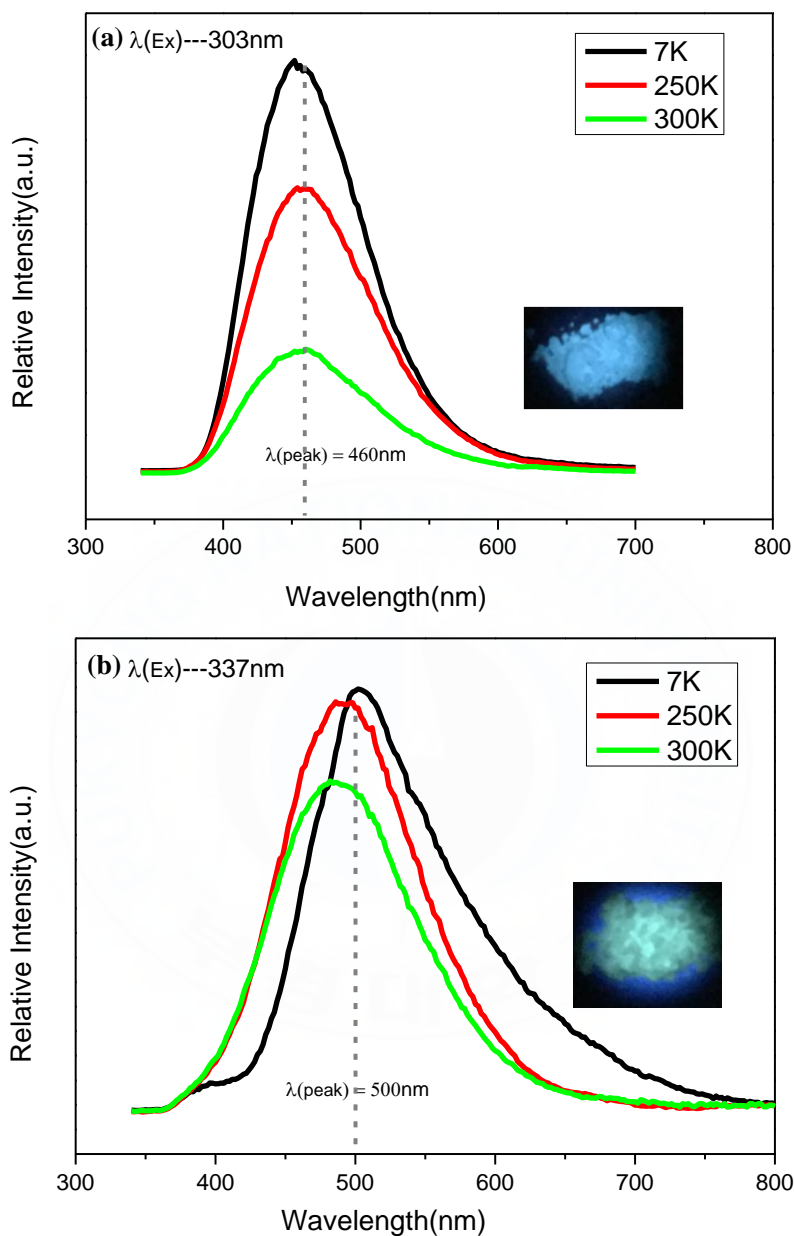


Fig. 4.1.6 Emission spectrum of Y_2WO_6 crystal at the temperature of 7, 250 and 300 K. (a) excited by 303 nm; (b) excited by 337 nm.

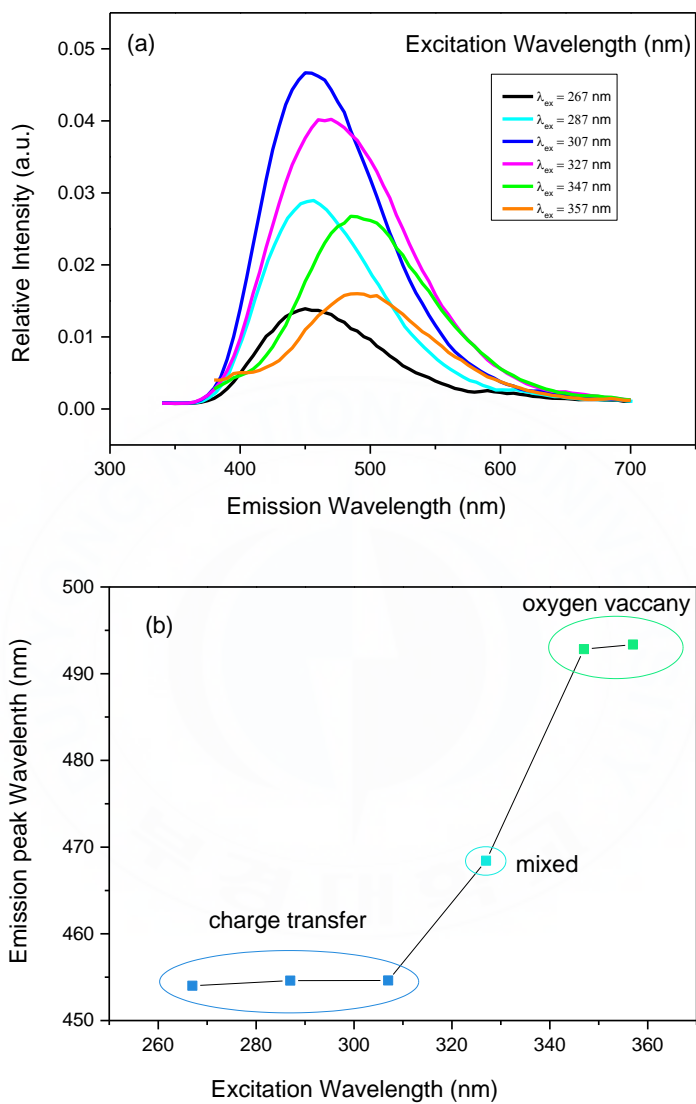


Fig.4.1.7 (a) Emission spectrum of Y_2WO_6 excited by different wavelength at 300K. (b) The emission peak position as a function of excitation wavelength.

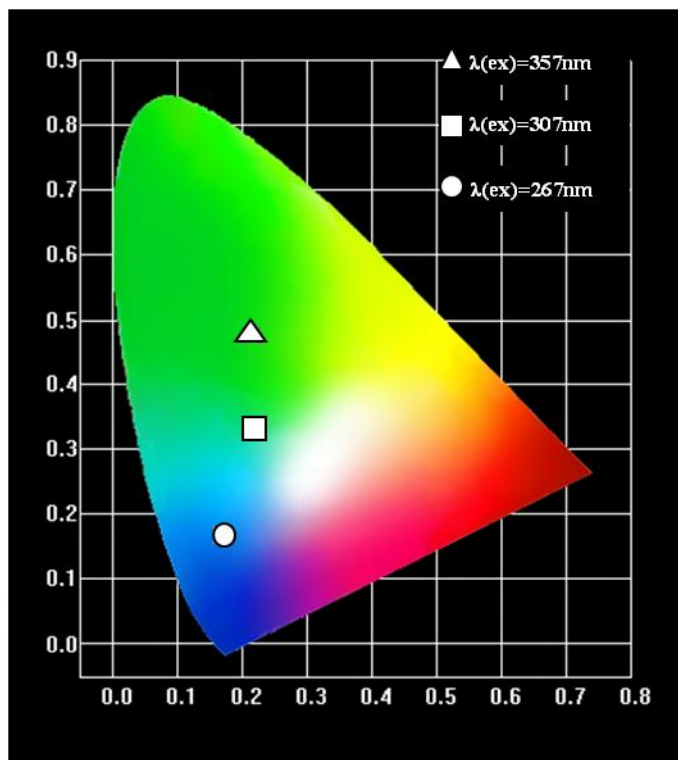


Fig.4.1.7 CIE chromaticity diagram showing color coordinates of the luminescence excited by different wavelength.

The above mentioned results indicate that the self-activated luminescence of the Y_2WO_6 crystal is changed from blue to green depending on the excitation wavelength due to the possession of two types of luminescent centers. To further clarify the relationship between the emission properties and excitation wavelength, the measurement at different excitation wavelength was performed at room temperature. Emission spectrum of Y_2WO_6 in Fig. 4.1.7 (a) shows the peak position shifts to longer wavelength direction as the excitation wavelength

increases. The change in peak position with excitation wavelength shows in Fig. 4.1.7 (b) and the CIE color coordinates of the luminescence in Fig. 4.1.8. It is obvious that the emitting color shifts from blue to bluish and at last to pure green.

The origin of luminescence centered at 490 nm can be explained by excitation spectra as shown in Fig. 4.1.8. Even at 300 K, the excitation spectra of hydrothermal sample show the two distinct peaks but it cannot be observed at the spectra at 300 K for the solid state sample. We realized that the crystallinity of hydrothermal sample is better than the solid state sample according to the XRD patterns as shown in Fig. 4.1.1. So it is reasonable that there exist more amount of oxygen vacancy in the hydrothermal sample. Thus the luminescence center is suggested to be due to the oxygen vacancy.

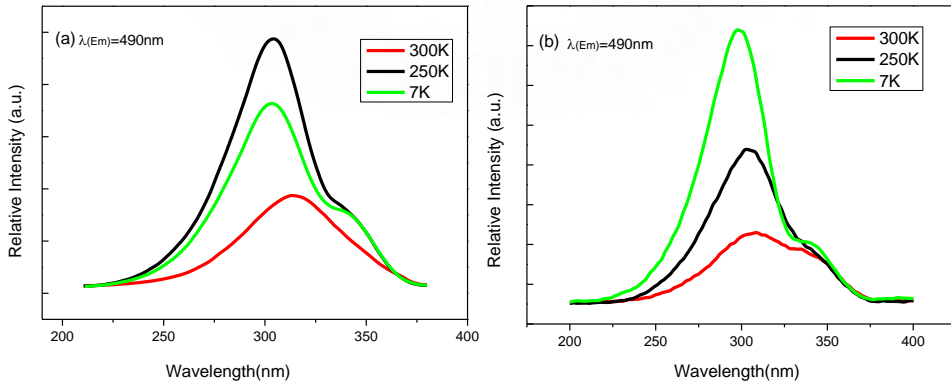


Fig. 4.1.8 Excited spectrum of Y_2WO_6 crystal monitored the 490 nm at 7, 100 and 300K. (a) solid state method; (b) hydrothermal method.

4.2 Upconversion luminescence of $Y_2WO_6:Yb^{3+}/Er^{3+}$

4.2.1 Morphology and structure

The XRD patterns were measured to confirm the crystal structure of the samples. As shown in Fig.4.2.1, the profiles of the XRD patterns are almost the same except for slight shift of peaks. By increasing Er^{3+} concentration from 0.001% to 20% the peaks shift to lower angles since the ionic radius of Er^{3+} is slightly smaller than that of Y^{3+} ionic radius. All of the peaks are found to be well matched with JCPDS: No.23-1489 card as shown in Fig. 4.2.1 (a). It was found no heterogeneous diffraction peaks belonging to other compounds beyond Y_2WO_6 monoclinic phase. This indicates that the $Y_2WO_6:10\%Yb/x\%Er$ phosphors were synthesized successfully by solid state method and the crystal lattice keeps its own monoclinic phase after doping rare earth ions with different concentration.

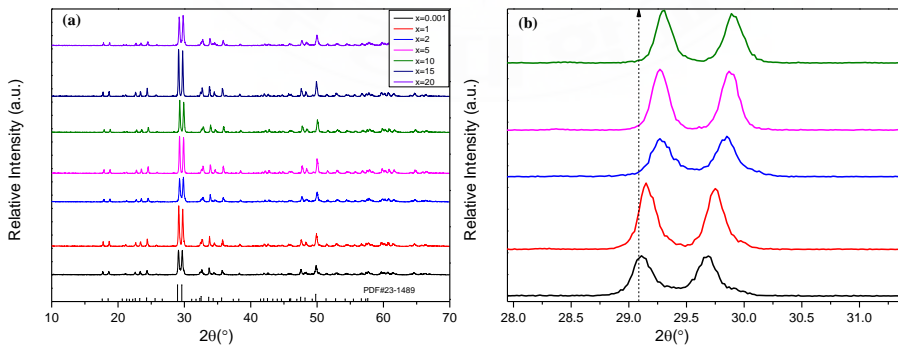


Fig. 4.2.1 XRD patterns of $Y_2WO_6:10\%Yb/ x\%Er$ phosphors with various (from 0.001% to 20%) Er^{3+} concentration (b) Diffraction peaks shift as Er^{3+} concentration increasing.

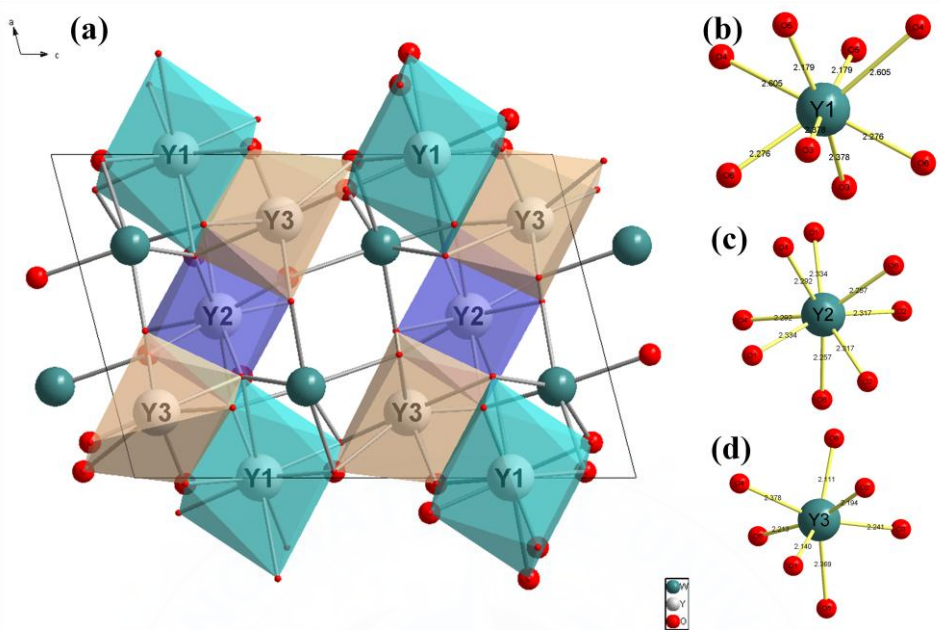


Fig.4.2.2 (a) Sketch map of monoclinic Y_2WO_6 crystal structure in the $P 1 2/c 1$ (13) space group. (b) Three kinds of different Y-O coordination polyhedron link through edge-sharing. (c) (d) and (e) Three kinds of different Y-O coordination, respectively.

The Y_2WO_6 crystal structure (Yttrium oxytungstate, or $Y_2O_3 \cdot WO_3$) was reported by Borchardt for the first time in 1963[26]. There exist three different kinds of space groups of crystal structure of yttrium oxytungstate: $P2_12_12_1$, $P4/nmm$ and $P12/c1$ (there are two polymorphs with two different unit cells in the space group of $P2_12_12_1$), which could be found in the Inorganic Crystal Database (ICSD) [27-30]. Fig. 4.2.2 is a sketch diagram to illustrate organization form of monoclinic Y_2WO_6 structure.

The crystal structure was built using a software package (Diamond 3.2, Crystal and Molecular Structure Visualization) based on the crystal structure database. The position of Y(1), Y(2) and Y(3) sites was shown in Fig. 4.2.2 (a). It can be seen that two of them were coordinated by 8 oxygen atoms and the other was coordinated by 7 atoms. Y^{3+} occupies three sites in the crystalline lattice with the different bond length and bond angle. Three kinds of polyhedrons were formed and linked mutually via sharing the same edge. The shape of polyhedron, the Y-O coordinate atoms of Y(1), Y(2) and Y(3) was showed in Fig. 4.2.2 (b) (c) and (d). We also observe from sketch map that W^{6+} is different from Y^{3+} , each of the W^{6+} ions is surrounded by 6 O^{2+} ions and the W-O octahedrons were built. The doped rare earth Er^{3+} and Yb^{3+} randomly substitutes for the three Y^{3+} crystallographic sites. The atomic radii of Yb (176 pm, empirical, the same below) and Er(176 pm) to the Y(180 pm) rather than the atomic radiu of the W (139 pm) atoms.

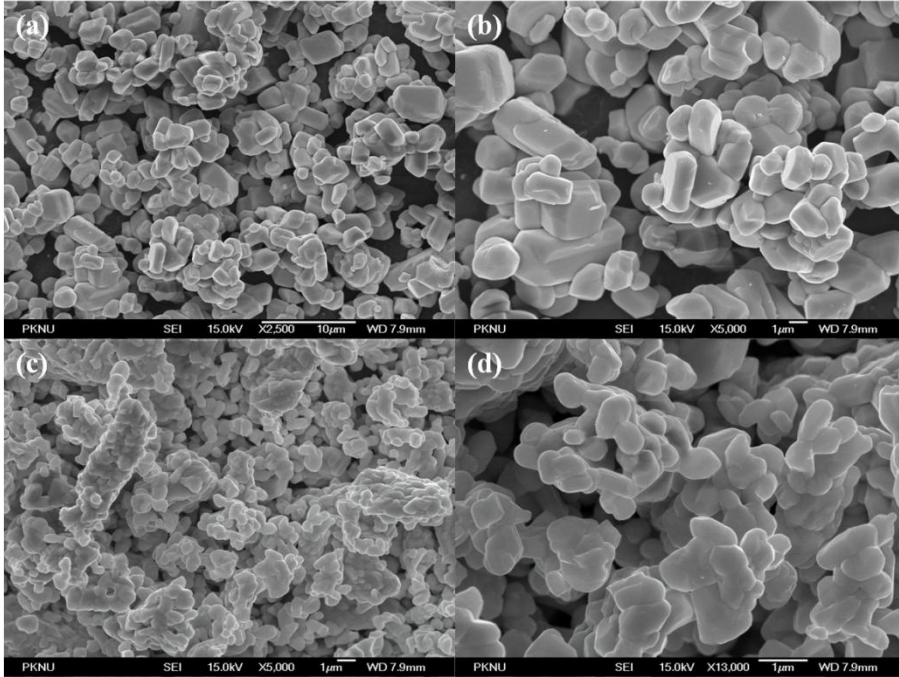


Fig. 4.2.3 The SEM images of Y_2WO_6 co-doped with 10%Yb and 2% Er (a) (b) and 10% Yb and 20% Er (c) (d) at different magnification synthesized by solid state method.

The shape and size of the solid state phosphors are observed in the FE-SEM and the representative SEM images as shown in Fig. 4.2.3. The sample of $Y_2WO_6:10\%Yb^{3+}/2\%Er^{3+}$ phosphors was synthesized in a slow temperature rising rate and short temperature holding time. The completely grinding was performed for several times at sintering temperature of 700, 900, 1100 and 1200 °C and then the final phase formed. The phosphor particles are quite well crystallized with a few micrometers in size and the uniform size distribution. Fig. 4.2.3 (a) (b)

exhibits approximately rhomb with clear edges, which accord with its monoclinic phase characterization. The shape difference between (a) (b) and (c) (d) indicates that the temperature rising rate, temperature holding time and the number of times of grinding are important conditions for acquiring the even morphologies.

4.2.2 Luminescence properties

It is well known that the most considerable factor affecting the luminescent performance is the doping concentration of luminescence centers in luminescence materials. The dependence of upconversion luminescence properties on Er^{3+} concentration was investigated for $\text{Y}_2\text{WO}_6:10\% \text{Yb}^{3+}/x\% \text{Er}^{3+}$. Fig. 4.2.4 shows upconversion emission spectrum of the sample series under 980 nm excitation with various Er^{3+} concentration which Yb^{3+} concentration was fixed to be 10%.

The emission bands of Er^{3+} are observed at 410nm (${}^2\text{H}_{9/2} \rightarrow {}^4\text{I}_{15/2}$), 480 nm (${}^4\text{F}_{7/2} \rightarrow {}^4\text{I}_{15/2}$), 530 nm (${}^2\text{H}_{11/2} \rightarrow {}^4\text{I}_{15/2}$), 550 nm (${}^4\text{S}_{3/2} \rightarrow {}^4\text{I}_{15/2}$), 665 nm (${}^4\text{F}_{9/2} \rightarrow {}^4\text{I}_{15/2}$), 867 nm (${}^4\text{I}_{9/2} \rightarrow {}^4\text{I}_{15/2}$). The visible upconversion emissions at green and red bands are stronger in the spectrum. Meanwhile, blue and near infrared emissions are also observed with weak intensity. The integrated emission intensities were calculated from the emission spectrum in Fig. 4.2.4 (a) and the results were shown in Fig. 4.2.4 (b). The integrated emission intensity increases up to the concentration of 2% and then decreases.

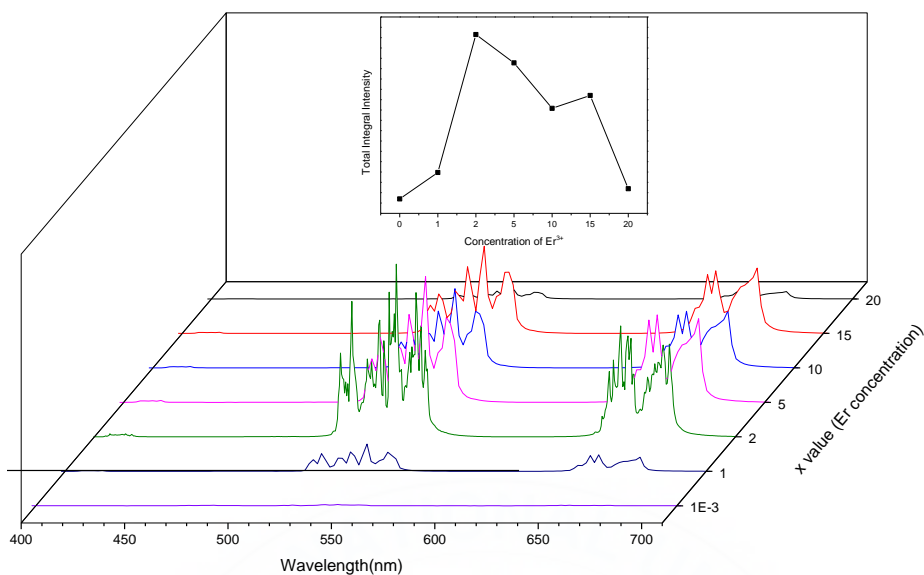


Fig. 4.2.4 Concentration dependence of upconversion emission spectrum of $\text{Y}_2\text{WO}_6:10\%\text{Yb}^{3+}/x\%\text{Er}^{3+}$ under 980 nm excitation; The inset: the relationship between integrated upconversion emission intensities and Er^{3+} concentration;

It is concluded that optimal concentration (or quenching concentration) to realize most intense upconversion luminescence is 2%. It is worthy to note that all the samples with various doping concentration show very bright green light even for extremely low Er^{3+} concentration.

The quenching mechanism is depicted in details in Fig. 4.2.5. When the sample is excited by 980 nm laser diode, the energy level $^4\text{F}_{7/2}$ is populated through energy transfer (ET) and excited state absorption (ESA) process [31-34]. The energy level of $^4\text{F}_{7/2}$ is mainly populated by ESA for lower Er^{3+} concentration. However, the ET processes between Er^{3+} ions

and between Yb^{3+} and Er^{3+} ions become the main approach to populate [35] as the Er^{3+} concentration increases. The populations of the $^4\text{F}_{7/2}$ level would increase as Er^{3+} concentration increases, for the reason that it is in relation to inverse proportional between the energy transfer rates and the average distance between the rare earth ions.

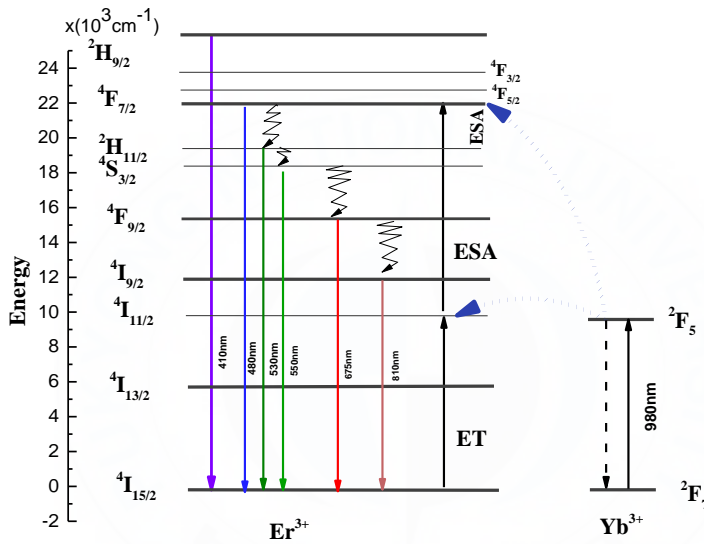


Fig. 4.2.5 Excitation and emission routes of upconversion process und980-nm excitation in the $\text{Y}_2\text{WO}_6:10\% \text{Yb}/x\% \text{Er}$ phosphors

Power dependence of upconversion emission spectrum Figs.4.2.5 (a) and (b) show the upconversion emission of Er^{3+} and Yb^{3+} codoped Y_2WO_6 crystals in the visible region excited by continuous wave 980 nm laser diode under different laser power at room temperature. The peaks are assigned to the following transitions: the band of 500 - 580 nm (the green band) to the $(^2\text{H}_{11/2}, ^4\text{S}_{3/2}) \rightarrow ^4\text{I}_{15/2}$ transition, and the 630 -700 nm band to

the ${}^4F_{9/2} \rightarrow {}^4I_{15/2}$ transition. Additionally, Fig. 4.2.5 (b) shows magnified spectrum of the part in black-dashed rectangle of (a) in which the other three peaks are observed even it is very weak. The three peaks are due to the ${}^4F_{7/2} \rightarrow {}^4I_{15/2}$, ${}^4H_{7/2} \rightarrow {}^4I_{15/2}$ and ${}^2H_{9/2} \rightarrow {}^4I_{15/2}$ transitions of Er^{3+} centered at 867, 480 and 410 nm, respectively. The excitation and emission routes of the system are shown in Fig. 4.2.6.

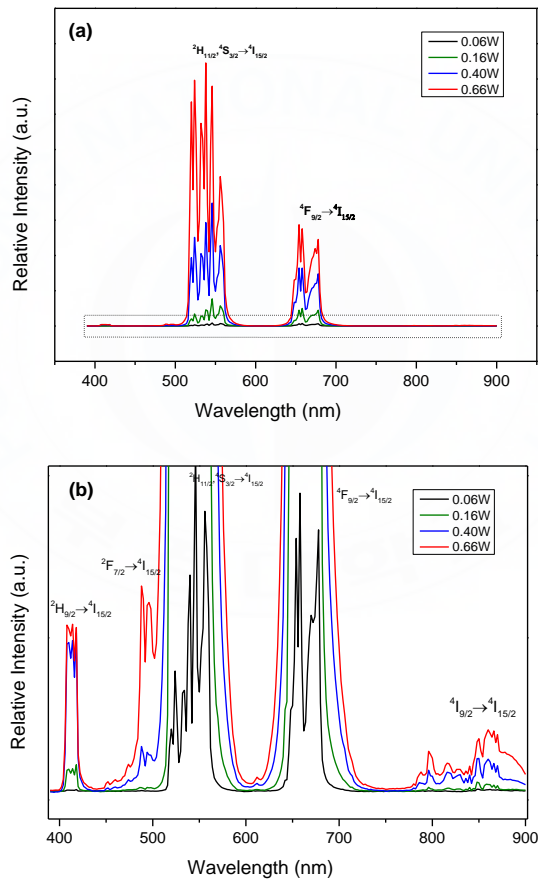


Fig. 4.2.5 (a) Upconversion emission spectrum of the sample $\text{Y}_2\text{WO}_6:10\%\text{Yb}/2\%\text{Er}$ excited by 980nm LD under different

power. (b)The partial emission spectrum of (a) marked by black-dashed rectangle.

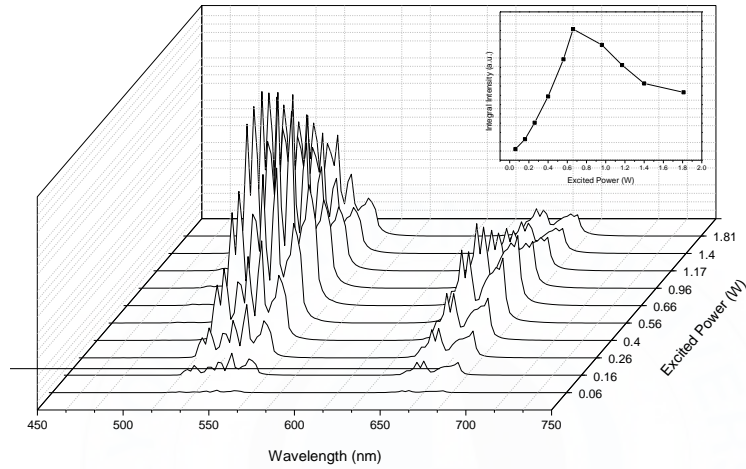


Fig. 4.2.7 Power dependence of upconversion emission spectrum of the sample $Y_2WO_6:10\%Yb/2\%Er$ excited by 980nm LD. The insert plot is integral intensity under different power excited.

To better understand the upconversion mechanism of the sample $Y_2WO_6:10\%Yb/x\%Er$, the upconversion luminescence intensity of the green and red emission bands as a function of pump power was measured. Fig. 4.2.7 shows the power dependence of upconversion emission spectrum of the sample $Y_2WO_6:10\%Yb/2\%Er$ excited by 980 nm laser

diode. The emission intensity increases rapidly at first, after its maximum value it begins to decrease. The insert in Fig. 4.2.7 shows calculated integral intensity which clarifies the variation tendency of luminescence intensity as a function of excitation power.

Fig. 4.2.8 shows the logarithmic plot of the integrated emission intensities of the upconversion emission red and green band as a function of incident power density. The samples are excited by 980 nm and the $^2H_{11/2}/^4S_{3/2}$ levels are populated via excited state absorption and energy transfer process. The output slopes (n) for green band (500 to 580 nm) for various Er^{3+} doping concentration are 1.77, 2.14, 2.03, 1.73, 1.74, 1.47 and 1.74 as shown in Fig. 4.2.8. This indicates that the two photon processes are responsible for the population of $^4F_{7/2}$ energy level of Er^{3+} . It is interesting to find the decrease trend of slope values with the Er^{3+} concentration in a range from 1 to 15% as shown in Fig. 4.2.8 (c). The reason is that the cross relaxation interactions between Er^{3+} begin to take effect as the Er^{3+} concentration increases. The possible cross relaxation routes CR1, CR2 and CR3 are illustrate in Fig. 4.2.9. The cross relaxation rates are inversely proportional to the average distance between Er^{3+} ions, thus they would increase greatly with increasing Er^{3+} concentration, and the emission intensity of Er^{3+} would decrease. So the slope value decreases because of the competition between the cross relaxation and the upconversion processes as the Er^{3+} concentration increases. In addition, the downtrend of slope value is also similar for red emission for the reason that the transition of $^4F_{9/2}$ level is also influenced by the cross relaxation

process (see Fig. 4.2.8 (b)). We note that the slope values of red band are less than that of the green.

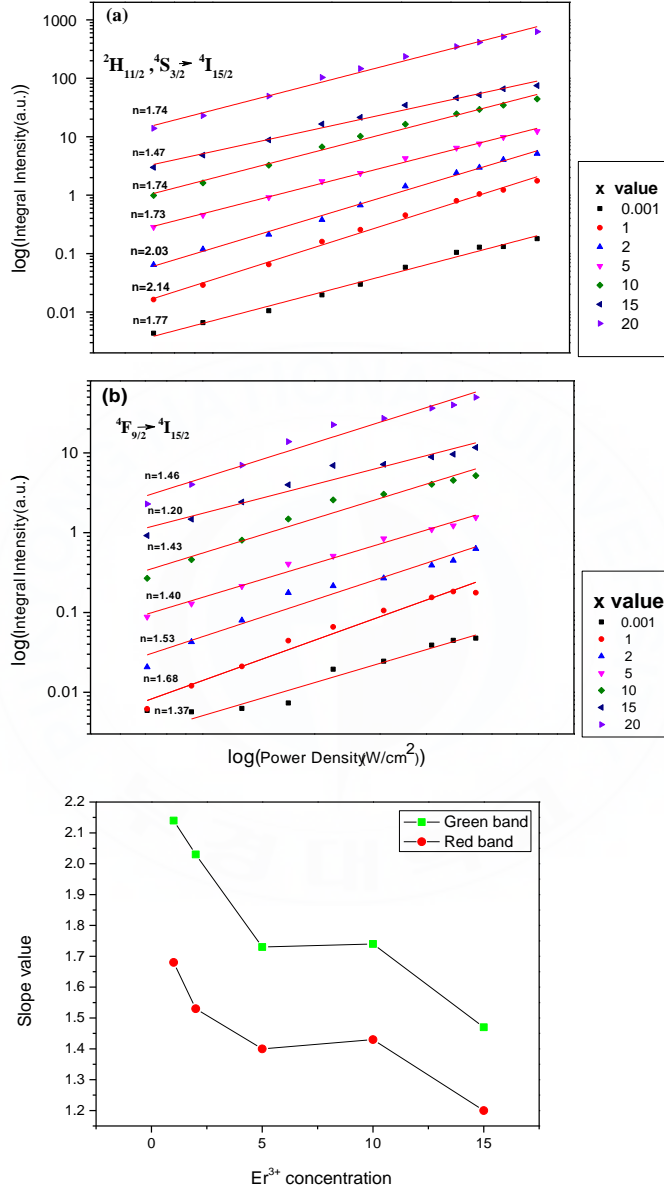


Fig. 4.2.8 Log-log plot of the integral intensity as a function of the pump power for various Er³⁺ concentration. (a)Green band

4.3 Upconversion properties of $\text{Y}_2\text{WO}_6:10\%\text{Yb}^{3+}/2\%\text{Er}^{3+}$

4.3.1 Structure and morphology

$\text{Y}_2\text{WO}_6:10\%\text{Yb}^{3+}/2\%\text{Er}^{3+}$ was synthesized via a facial hydrothermal method at the presence of surfactant SDBS (sodium surfactant dodecyl benzene sulfonate) and then the precursors were annealed at higher temperature for 4 hours to obtain the final products. The yttrium tungstate could not be synthesized directly in the solutions [36]. Fig. 4.3.1 shows XRD patterns of hydrothermal products at annealing temperature 700, 850 and 950 °C.

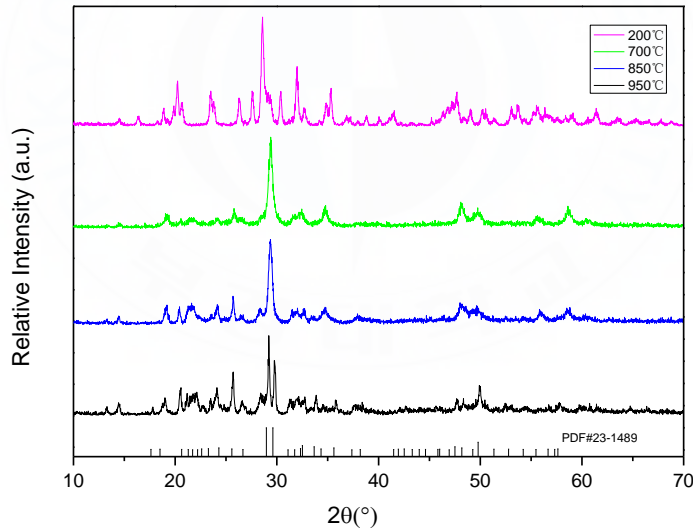


Fig. 4.3.1 XRD patterns of $\text{Y}_2\text{WO}_6:10\%\text{Yb}/2\%\text{Er}$ phosphors synthesized by hydrothermal method. (precursors and annealing at the temperature of 700°C, 850 °C, 950 °C)

As seen in Fig. 4.3.1, there exist many impurity peaks in the XRD patterns of the precursor samples. After annealing at 700 °C, the majority of impure peaks were disappeared but still not very well crystallized. Peaks in low diffraction angle occurred when temperature increase to 850 °C. A monoclinic Y_2WO_6 phase is formed with obvious characteristic peaks when the heat treatment was carried out at 950 °C.

It is worthy to note that the pH value is the most crucial factor to synthesis the samples. The pH value must be adjusted to neutral for obtaining the expectant products. Other impure phases can be formed through the hydrothermal process when the pH value is not appropriate. For example, the yellow-green particles of WO_3 are formed when the pH value is lower than 2, since the ions tend to mutually combined to precipitate with specific stoichiometric ratio in the specific pH value in solution.

The samples were synthesized at the presence of 1 mmol of SDBS and neutral pH value. The pH value is vital factors to affect the nucleation and growth during the hydrothermal processes. The surfactant SDBS is organic molecule hydrophobic tail and hydrophilic head, which can be formed micelle in an appropriate concentration in solution [37]. The hydrophilic part of the molecule extends to the solution while the hydrophobic tails gather together. The micelle in the substrate solution could be influential factor to tune the morphology of the hydrothermal precursors.

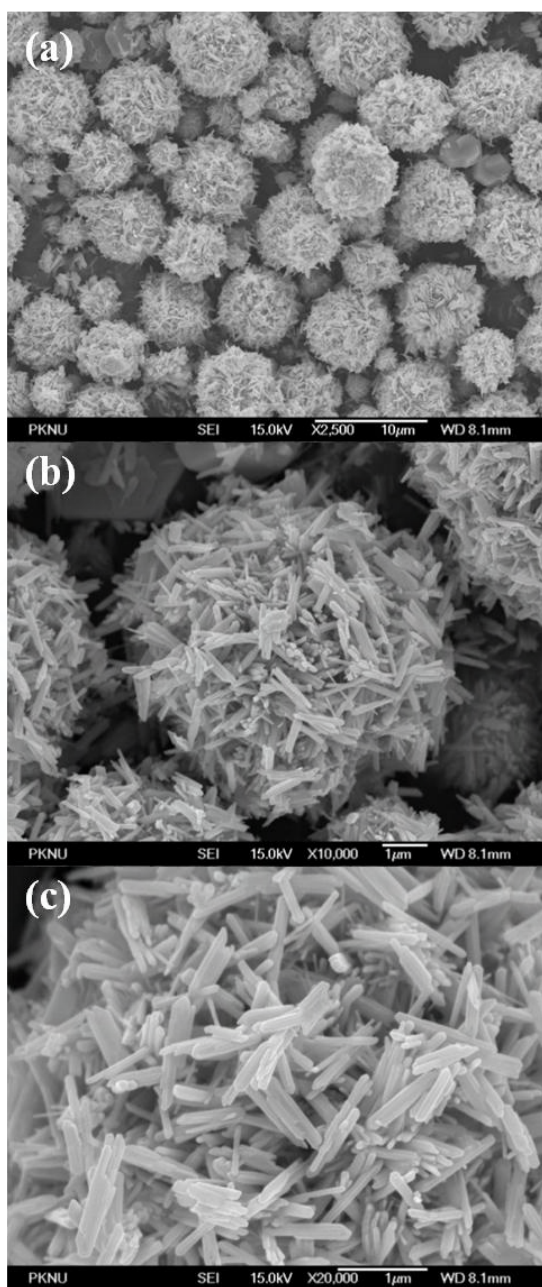


Fig.4.3.2 SEM images of Y_2WO_6 precursors co-doped with 10% Yb and 2% Er synthesized by hydrothermal method at different magnification.

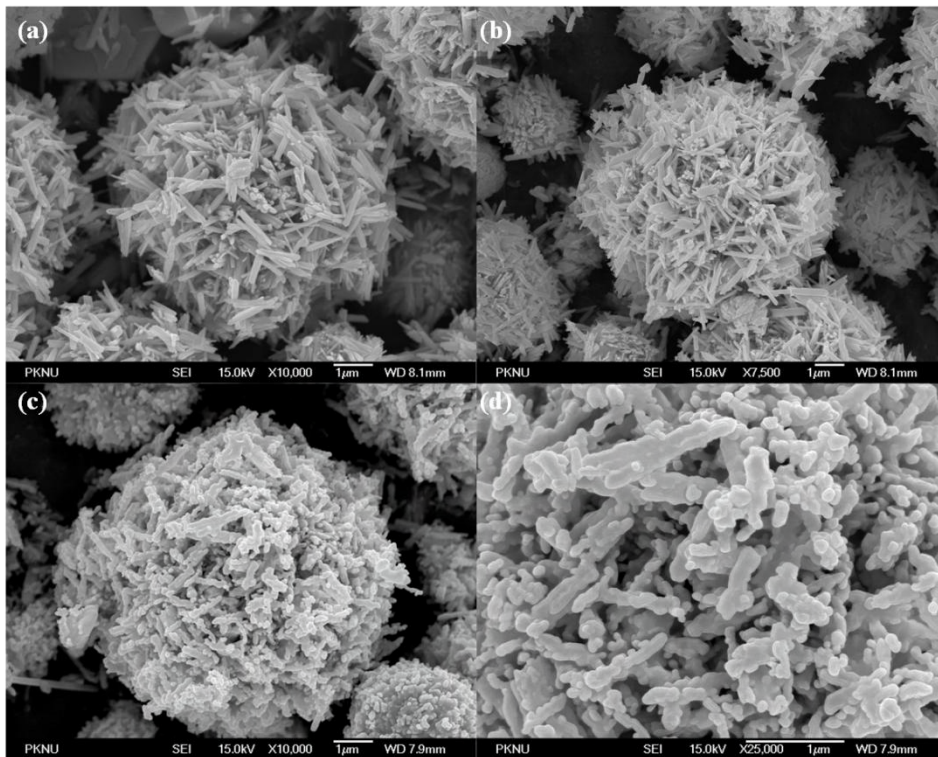


Fig.4.3.3 FE-SEM images of $Y_2WO_6:10\%Yb^{3+}/Er^{3+}$ synthesized by hydrothermal method and the pH value is 6.0. (a)precursors; (b)annealing at $700\text{ }^\circ\text{C}$; (c)annealing at $950\text{ }^\circ\text{C}$; (d) Enlarged images of (c).

The FE-SEM photographs in Fig. 4.3.2 and Fig. 4.3.3 exhibit the morphology characteristics of $Y_2WO_6:10\%Yb^{3+}/2\%Er^{3+}$ precursors. The sample grew into the needle-shaped products with about $1\text{ }\mu\text{m}$ at the presence of surfactant SDBS and at the pH value 6.5. A mass of needles aggregated into the spheres with the radius approximately a few

micrometers (see Fig.4.3.2). When we took heat treatment at 700, 850, and 950°C for improving the crystallinity, the superficial morphology of the samples also changes as the temperature increases. The samples keep its needle-shaped morphology with clear edge annealed at 700°C but the luminescence performance is different compared with the hydrothermal precursor, detailed description in Fig. 4.3.7. The morphology changes when temperature increases up to 950°C. The edge of the needle is not clear anymore because some needles melt together. However, particles still keep its original size.

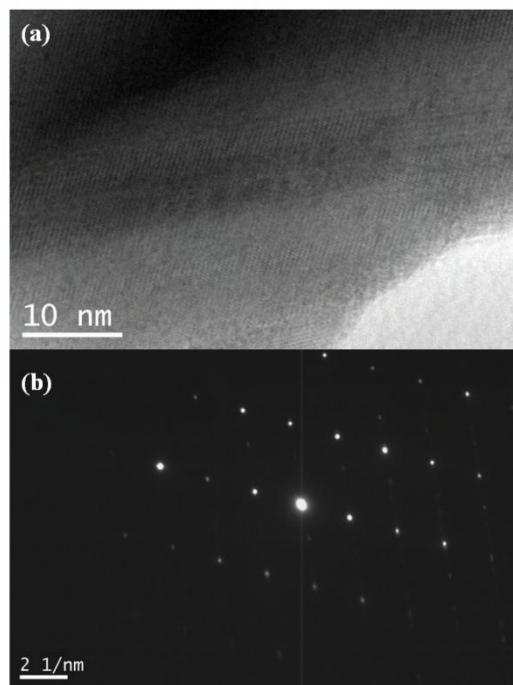


Fig.4.3.4 HR-TEM images of $\text{Y}_2\text{WO}_6 : 10\% \text{Yb}^{3+} / 2\% \text{Er}^{3+}$.

The sample of Y_2WO_6 codoped 10% Yb^{3+} and 2% Er^{3+} also characterized by HR-TEM. The diffraction image in the selected area in Fig. 4.3.4 (b) confirms the single crystallinity nature of the Y_2WO_6 samples.

4.3.2 Luminescence properties

Fig. 4.3.5 shows the upconversion emission spectrum of $\text{Y}_2\text{WO}_6:10\%\text{Yb}^{3+}/2\%\text{Er}^{3+}$. All the peaks are involved in the strong green band, the strong red band and the other weak blue and infrared band which are the same as observed for the samples by solid state method (see Fig.4.3.5 insert). The emission band of Er^{3+} exhibits rich lines due to the transitions together with weak broad band of host lattice (see Fig.4.3.6). The reason is speculated as the influence of the host structure. The products by hydrothermal process at different annealing temperature show the different crystallinity. In this work it is convenient to further investigate the influence of crystal structure on the luminescence properties.

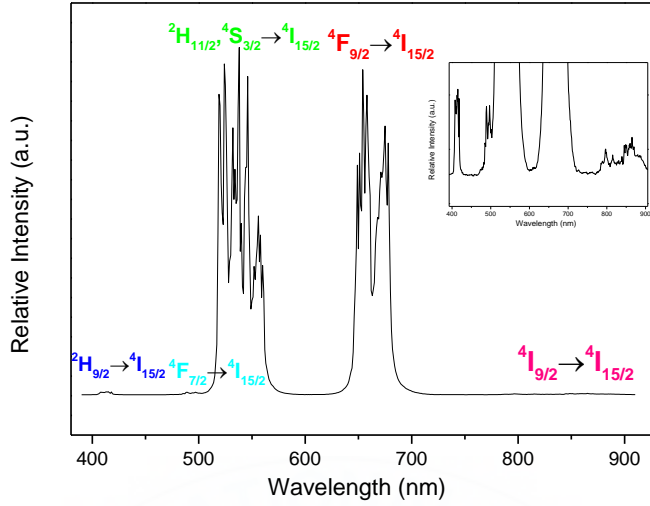


Fig. 4.3.5 Upconversion emission spectrum of the Y_2WO_6 co-doped with 10% Yb^{3+} and 2% Er^{3+} . Insert plot is enlarged part of the weak peak.

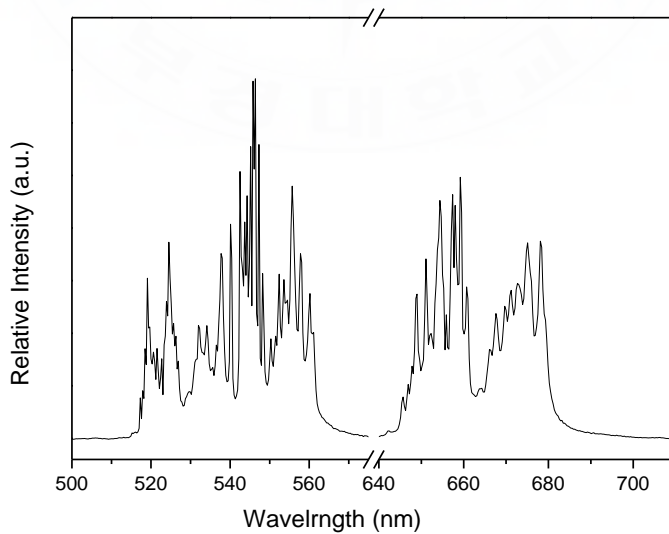


Fig.4.3.6 The phenomenon of severely split in the emission band.

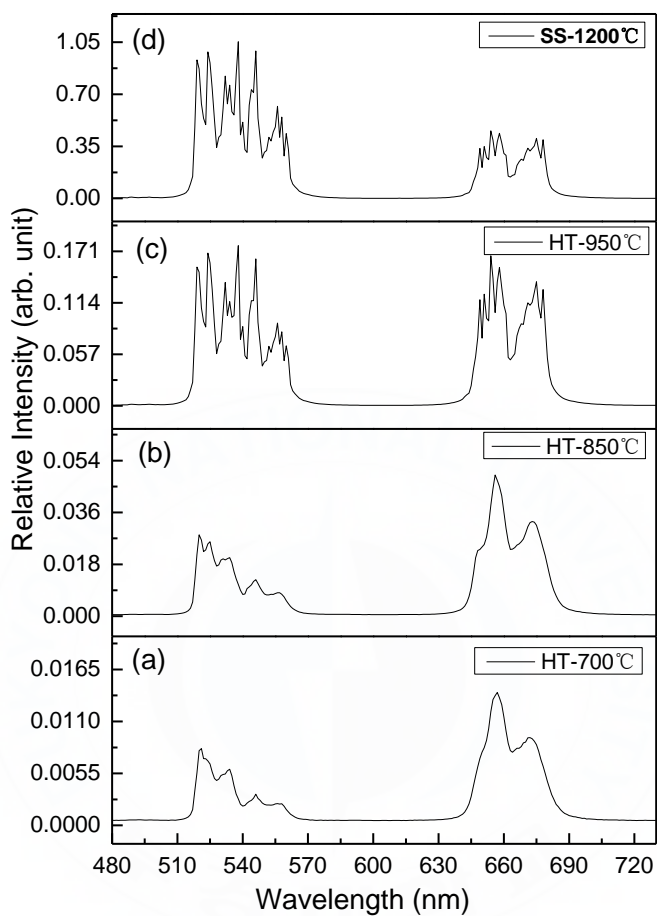


Fig. 4.3.7 Upconversion emission spectrum of the $\text{Y}_2\text{WO}_6:10\%\text{Yb}^{3+}/2\%\text{Er}^{3+}$. (a) Synthesized by hydrothermal and annealing at 700 °C; (b) synthesized by hydrothermal and annealing at 850 °C; (c) synthesized by hydrothermal and annealing at 950 °C; (d) synthesized by solid state method at 1200 °C

Fig. 4.3.7 shows the luminescence properties of hydrothermal products at different annealing temperatures. The peaks in the emission spectrum broaden at the annealing temperature of 700 and 850 °C. The spectral shape of the emission band is similar between 700 and 850 °C and the emission intensity is stronger for 850 °C. The emission band split into many sharp peaks when the sample is annealed at 950 °C. It is found from XRD results that the sample is well crystallized at 950 °C but the diffraction peaks are still broad and unclear at 850 °C. The splitting in the emission band is elucidated by comparing the XRD results and spectral feature. It needs further investigation to explain the relationship between the peak splitting and crystal structure. The crystallinity is not very well when the precursors are annealed at low temperature, i.e. the internal structure of phosphors in atomic array is still disordered. It indicates that the local surroundings of Er^{3+} is irregular but isotropic so that the band does not split severely. As the temperature increases, the atomic order in crystal becomes organized. The regular coordination environment leads to three different kinds of Er^{3+} sites, i.e. Er^{3+} ions is influenced by different crystal field strength. Therefore, the emission spectrum of Y_2WO_6 codoped with 10% Yb^{3+} and 2% Er^{3+} is split severely.

4. Conclusion

The monoclinic yttrium tungstate Y_2WO_6 was synthesized by different method: solid state and hydrothermal approaches. The structure and morphology, excitation and emission spectrum were measured to investigate luminescence properties. The emitting color of the sample is tunable by variational excitation wavelength due to the existence of two different luminescent centers. It is originated that the peak located at 460 nm from the W-O charge transfer and the peak located at 500 nm from oxygen vacancy.

The upconversion luminescence properties of Y_2WO_6 co-doped 10% Yb^{3+} and x% Er^{3+} were investigated in this work. The samples with particular morphology were obtained due to the presence of surfactant SDBS. The samples were characterized by XRD, SEM, excitation and emission spectra and they show characterized optical properties. The slope values of the power dependence decrease as the Er^{3+} concentration increases for the reason of the cross relaxation process. In addition, the severely splitting phenomenon in spectrum was observed because of the diverse Er^{3+} sites.

Acknowledgement

The work of luminescence properties study presented in my thesis was executed in the Laboratory of Luminescent Materials, belonging to Interdisciplinary Program of Biomedical Engineering, Pukyong National University.

I would like to express my gratitude to all the people who gave me help during the process of prepared the thesis and my whole master learning process.

First of all, I am so gratefully to my supervisor, Prof. Hyo Jin Seo who offered me insightful suggestions for both my academic study and my ordinary life. Prof. Seo spent much time for me to communicate my opinions, provided inspiring advice and discussed experiment results. It is impossible for me to complete my thesis without the expert and patient guidance from Prof. Seo.

I would like to express my deep thanks to Prof. Yanlin Huang who was greatly encouraged me when I suffered setbacks and told me people should live an aspiring life. Prof. Huang paid much attention to my academic study, helped me a lot with his extensive knowledge and gave me good opportunities to improve myself.

It is to show my sincere appreciate to all of my kind-hearted lab-mates and friends. Prof. Xipeng Pu, Dr. Peiqing Cai, Dr. Lin Qin, Han Cheng, Hang Dang Thi, Quynh Vu Thi and Jing Wang, who always try

their best to help me work out the problems encountered in daily life or study work. I have a wonderful life in Busan because of them.

At last, I would express my gratitude to my beloved families for their continuously support and encouragement during all my life.



Published Papers

- [1] Guan Y, Huang Y, Tsuboi T, Huang W, **Chen C**, Cai P and Seo H J 2014 Conversion and quantum efficiency from ultraviolet light to near infrared emission in Yb^{3+} -doped pyrovanadates MZnV_2O_7 (M= Ca, Sr, Ba) *Materials Science and Engineering: B* 190 26-32
- [2] Lu Y, Chen L, Huang Y, **Chen C**, Kim S I and Seo H J 2015 Layer structured $\text{Na}_2\text{Ni}(\text{MoO}_4)_2$ particles as a visible-light-driven photocatalyst for degradation of methylene blue *Applied Surface Science* 331 72-8
- [3] Lu Y, Pu Y, Wang J, Qin C, **Chen C** and Seo H J 2015 On structure and methylene blue degradation activity of an Aurivillius-type photocatalyst of $\text{Bi}_4\text{V}_2\text{O}_{11}$ nanoparticles *Applied Surface Science* 347 719-26
- [4] Meng F, Zhang H, **Chen C**, Kim S I, Seo H J and Zhang X 2016 A study of luminescence from Eu^{3+} , Ce^{3+} , Tb^{3+} and $\text{Ce}^{3+}/\text{Tb}^{3+}$ in new potassium gadolinium phosphate $\text{K}_3\text{Gd}_5(\text{PO}_4)_6$ *Journal of Alloys and Compounds* 671 150-6
- [5] Pu Y, Huang Y, Qi S, **Chen C** and Seo H J 2015 In situ hydroxyapatite nanofiber growth on calcium borate silicate ceramics in SBF and its structural characteristics *Materials Science and Engineering: C* 55 126-30
- [6] Pu Y, Huang Y, Tsuboi T, Huang W, **Chen C** and Seo H J 2015 An

- efficient yellow-emitting vanadate $\text{Cs}_5\text{V}_3\text{O}_{10}$ under UV light and X-ray excitation *Materials Letters* 149 89-91
- [7] Pu Y, Wang J, Huang Y, **Chen C**, Kim S I and Seo H J 2015 Visible-Light-Induced Degradation of Methylene Blue by SrBi_3VO_8 Nanoparticles *Journal of the American Ceramic Society* 98 2528-33
- [8] Yang L, Wan Y, Huang Y, **Chen C** and Seo H J 2016 Development of $\text{YK}_3\text{B}_6\text{O}_{12}:\text{RE}(\text{RE}=\text{Eu}^{3+}, \text{Tb}^{3+}, \text{Ce}^{3+})$ tricolor phosphors under near-UV light excitation *Journal of Alloys and Compounds* 684 40-6
- [9] Zhang D, Pu X, Kim S I, Cai P, **Chen C** and Seo H J 2015 $\text{Na}_4\text{La}_{2-2x}\text{Tb}_{2x}(\text{CO}_3)_5$ nanophosphors: Hydrothermal synthesis and photoluminescence properties *Journal of Luminescence* 168 293-6
- [10] Zhang X, Zhang H, **Chen C**, Kim S I and Seo H J 2016 On the luminescence properties and site occupation of Ce^{3+} in new $\text{ScP}_2\text{O}_7(\text{A}=\text{Na}, \text{K})$ crystals *Materials Letters* 168 207-9

References

- [1] F. Auzel, C. R. Hebd, Seances Acad. Sci. 262 (15) (1966).1016
- [2] N. Bloembergen, Phys. Rev. Lett. 2 (3) (1959) 84.
- [3] F. Auzel, C. R. Hebd, Seances Acad. Sci. 263 (14) (1966) 819.
- [4] J. Reszczyńska, T. Grzyb, J. W. Sobczak, W. Lisowski, M. Gazda, B. Ohtani, and A. Zaleska, Appl. Catal. B 163 (2015) 40.
- [5] J. Wang, T. Wei, X. Li, B. Zhang, J. Wang, C. Huang, Q. Yuan, Angew. Chem. 126 (6) (2014) 1642.
- [6] F. Auzel, Chem. Rev. 104 (1) (2004) 139.
- [7] T. Grzyb, S. Balabhadra, D. Przybylska, M. Węclawiak, J. Alloys Compd. 649 (2015) 606.
- [8] T. Grzyb, A. Gruszczyńska, R. J. Wiglusz, Z. Śniadecki, B. Idzikowski, S. Lis, J. Mater. Chem. 22 (43) (2012) 22989.
- [9] T. Grzyb, A. Gruszczyńska, R. J. Wiglusz, S. Lis, J. Mater. Chem. C. 1 (34) (2013) 5410.
- [10] X. Wei, P. Geng, C. Han, Y. Guo, X. Chen, J. Zhang, Y. Zhang, D. Sun, S. Zhou, Ind. Eng. Chem. Res. 55 (19) (2016) 5556.
- [11] G. Wiggins, "Up-Conversion Emissions of Er³⁺ Doped Gd₂(WO₄)₃ Phosphors," (2016).
- [12] A. Pandey, V. K. Rai, V. Kumar, V. Kumar, H. Swart, Sens. Actuators, B. 209 (2015) 352.
- [13] M. Yin, Y. Liu, L. Mei, M. S. Molokeev, Z. Huang, M. Fang, RSC Adv. 5(89) (2015) 73077.

- [14] J. Li, J. Sun, J. Liu, X. Li, J. Zhang, Y. Tian, S. Fu, L. Cheng, H. Zhong, H. Xia, *Mater. Res. Bull.* 48 (6) (2013) 2159.
- [15] A.M. Kaczmarek, K. Van Hecke, R. Van Deun, *Adv. Inorg. Chem.* 53 (18) (2014) 9498.
- [16] B. Ding, C. Han, L. Zheng, J. Zhang, R. Wang, Z. Tang, *Sci. Rep.* 5 (2015).
- [17] M. Pollnau, D. Gamelin, S. Lüthi, H. Güdel, M. Hehlen, *Phys. Rev. B.* 61 (5) (2000) 3337.
- [18] Y. Qu, X. Kong, Y. Sun, Q. Zeng, H. Zhang, *J. Alloys Compd.* 485 (1) (2009) 493.
- [19] C.K. Jørgensen, *Absorption spectra and chemical bonding in complexes*, Elsevier. (2015).
- [20] C.K. Jørgensen, *Modern aspects of ligand field theory*, North-Holland Pub. Co. (1971).
- [21] A. Lever, *Inorganic electronic spectroscopy* 2, (1984) 376.
- [22] J.A. Duffy, *Bonding energy levels and bands in inorganic solids*, Longman (1990).
- [23] G. Blasse, *Structure and Bonding*, Springer Berlin. (1980)
- [24] W. Barendswaard, J. Van der Waals, *Mol. Phys.* 59 (2) (1986) 337.
- [25] J.S. Chivian, W. Case, D. Eden, *Appl. Phys. Lett.* 35 (2) (1979) 124.
- [26] H.J. Borchardt, *J. Chem. Phys.* 39 (3) (1963) 504.
- [27] V. Efremov, A. Tyulin, V. Trunov, O. Kudin, V. Yanovskij, V. Voronkova, *Kristallografiya* 28 (5) (1984) 904.
- [28] O. Beaury, M. Faucher, G. Teste de Sagey, *Acta Crystallogr. Sect. B:*

- Struct. Crystallogr. Cryst. Chem. 37 (6) (1981) 1166.
- [29] J. Huang, J. Xu, H. Li, H. Luo, X. Yu, Y. Li, J. Solid State Chem. 184 (4) (2011) 843.
- [30] A. Tyulin, V. Efremov, V. Trunov, Kristallografiya 34 (4) (1989) 885.
- [31] F. Auzel, Y. Chen, J. Lumin. 65 (1) (1995) 45.
- [32] Y. Liu, D. Tu, H. Zhu, R. Li, W. Luo, X. Chen, Adv. Mater. 22 (30) (2010) 3266.
- [33] Q. Meng, B. Chen, H. Zhong, J. Sun, L. Cheng, X. Zhang, M. Chen, J. Nanosci. Nanotechnol. 10 (3) (2010) 1895.
- [34] J.H. Chung, J.H. Ryu, J.W. Eun, J.H. Lee, S.Y. Lee, T.H. Heo, B.G. Choi, K.B. Shim, J. Alloys Compd. 522 (2012) 30.
- [35] J. Guo, F. Ma, S. Gu, Y. Shi, J. Xie, J. Alloys Compd. 523, (2012) 161.
- [36] A.M. Kaczmarek, Y.Y. Liu, P. Van Der Voort, R. Van Deun, Dalton Trans. 42 (15) (2013) 5471.
- [37] Y. Su, X. Xue, W. Xu, C. Liu, W. Xing, X. Zhou, T. Tian, T. Lu, Electrochim. Acta. 51 (20) (2006) 4316.